Magnetization Reversal in Submicron Disks: Exchange Biased Vortices

J. Sort,[1,*] A. Hoffmann,[2] S.-H. Chung,[2] K. S. Buchanan,[2] M. Grimsditch,[2] M. D. Baró,[1] B. Dieny,[3] and J. Nogués[4]

[1]*Departament de Física, Universitat Autònoma de Barcelona, 08193 Bellaterra, Spain*

[2]*Materials Science Division and Center for Nanoscale Materials, Argonne National Laboratory, Argonne, Illinois 60439, USA*

[3]*SPINTEC (URA 2512 CNRS/CEA), CEA/Grenoble, 17 Av. Martyrs, 38054 Grenoble Cedex 9, France*

[4]*Institució Catalana de Recerca i Estudis Avançats (ICREA) and Departament de Física, Universitat Autònoma de Barcelona, 08193 Bellaterra, Barcelona, Spain*

(Received 10 March 2005; published 1 August 2005)

Submicron, circular, ferromagnetic-antiferromagnetic dots exhibit different magnetization reversal mechanisms depending on the direction of the magnetic applied field. Shifted, constricted hysteresis loops, typical for vortex formation, are observed for fields along the exchange bias direction. However, for fields applied close to perpendicular to the exchange bias direction, magnetization reversal occurs via coherent rotation. Magnetic force microscopy imaging together with micromagnetic simulations are used to further clarify the different magnetic switching behaviors.

DOI: 10.1103/PhysRevLett.95.067201 PACS numbers: 75.60.Jk, 75.70.Cn, 75.75.+a

The rapid advancement in lithography methods for fabricating nanostructures with controlled dimensions and geometry has triggered increased research in magnetic nanostructures [1,2]. When the size of a magnetic element becomes of the same order as magnetic length scales, such as the domain wall width or the critical single domain size, the multidomain structure encountered in the bulk material becomes energetically unfavorable and either single domain or inhomogeneous magnetization configurations develop instead [1–4]. A case of particular interest is the formation of vortex states in circular or ring-shaped soft magnetic nanostructures [5–8]. When the Zeeman energy becomes sufficiently low, the magnetization curls up along the edges of the nanostructure to minimize the lateral stray fields, leading to a flux closure arrangement. This vortex formation results in a sudden drop of the magnetization at the so-called nucleation field. Towards the center of the vortex the magnetization turns out of plane, forming the vortex core. As the applied field is changed to negative saturation, the core moves perpendicularly to the field until it is expelled from the dot at the so-called annihilation field, where the vortex transforms back into a single domain [4].

In almost all magnetotransport devices, i.e., spin valves or tunnel junction structures, ferromagnetic (FM)—antiferromagnetic (AFM) exchange biased bilayers constitute an essential part [9]. Exchange bias, H_E, is defined as the shift of the hysteresis loop along the magnetic field axis typically observed in exchange coupled FM-AFM materials [10–13]. Many models attribute this effect to the formation of domains either in the FM or in the AFM layer [14–17]. Hence, apart from its crucial technological importance, the study of exchange bias in nanostructures is interesting from a fundamental point of view since the reduction of the lateral dimensions is likely to cause significant alterations to the domain structure of each layer [18–25].

In this Letter, we investigate the influence of the unidirectional FM-AFM coupling on the magnetization reversal of submicron circular Permalloy (Py)-IrMn dots. A constricted hysteresis loop (due to the formation of a vortex state), shifted along the magnetic field axis, is observed along the exchange bias direction. Beyond a critical angle the vortex no longer nucleates but, instead, the magnetization is found to reverse by ''coherent'' rotation of a so-called S state.

A continuous film with the composition Ta(5 nm)/Py(12 nm)/IrMn(5 nm)/Pt(2 nm) (where Py is FM and IrMn is AFM) was deposited onto a thermally oxidized Si wafer by dc magnetron sputtering. For comparison, a sample without the AFM, Ta(5 nm)/Py(12 nm)/Pt(2 nm), was also prepared. From the continuous films, arrays of circular dots with diameter of 400 nm and 800 nm periodicity were fabricated by e-beam lithography and subsequent ion etching [26]. For this geometry dipolar interactions are negligible [27]. To induce exchange bias, the as-prepared samples were field cooled (FC) from $T = 500$ K under an applied field of 3 kOe. Hysteresis loops were subsequently measured at room temperature with fields applied at several angles from the FC direction (which defines 0°), using a transverse magneto-optic Kerr effect (MOKE) setup. The magnetic configurations were investigated by magnetic force microscopy (MFM) under magnetic fields, in standard phase detection mode, with a lift height of 80 nm, using CoPtCr low moment probes. Micromagnetic simulations were performed using a Landau-Lifshitz-Gilbert micromagnetic solver [28] with saturation magnetization of bulk Py, $M_S = 8 \times 10^{-5}$ A/m, exchange stiffness constant $A = 1.05 \times 10^{-11}$ J/m, and using a cell size of approximately 6×6 nm^2. The magnetocrystalline anisotropy was neglected. The exchange bias field arising from the FM-AFM coupling ($H_E = 65$ Oe) was simulated as an additional static field, applied along 0°. Full hysteresis curves were calcu-

lated for external field directions ranging from 0° to 90° in plane.

The hysteresis loop of the circular uncoupled Py dots (without IrMn) is shown in Fig. 1(a). The constricted loop shape is typical of magnetization reversal via a vortex state [5–8]. For this sample, no significant differences in the shape of the loop were observed when measuring at different in-plane angles, indicating that the anisotropy of the FM and interdot dipolar interactions were negligible. Shown in Fig. 1(b)–1(e) are the hysteresis loops of the Py-IrMn dots measured along 0°, 75°, 80°, and 90° in-plane angles. The loop measured along 0° has a similar shape compared to the unbiased Py dots, suggesting that the magnetization reversal also occurs via vortex formation. However, the overall hysteresis curve is now shifted along the magnetic field axis by $H_E = 65$ Oe due to the coupling with the AFM. Note that the vortex state is still able to develop, although its formation may intuitively be energetically unfavorable due to the presence of a unidirectional coupling. Namely, during the cooling procedure a favored direction is set in the AFM. Thus, having FM spins at different angles from the FC direction, as it occurs in the vortex state, results in an increase of the exchange energy. Nevertheless, when the applied field effectively compensates the unidirectional coupling, the vortex state appears as the most energetically stable configuration.

When the measuring angle deviates from the FC direction, vortexlike hysteresis loops are still observed, up to an angle of 75° [see Fig. 1(c)]. However, beyond a critical angle, located between 75° and 80°, the hysteresis loops start to resemble hard axis loops, i.e., without constriction, indicating that the vortex no longer nucleates but, instead, the magnetization tends to reverse by coherent rotation [see Figs. 1(d) and 1(e)].

Selected MFM images corresponding to different values of the applied field, as indicated in the hysteresis loops of Fig. 1(b)–1(e), are shown in Fig. 2. The top left panel of Fig. 2(a) is the atomic force microscopy image of a single dot. On reducing the magnetic field from positive saturation along the FC direction, a dipolar contrast is observed at remanence [panel (i) in Fig. 2(a)]. This dipolar contrast progressively fades under application of negative fields, consistent with the nucleation of a vortex state, vanishing almost completely for an applied field $H_{\text{appl}} = -100$ Oe [panel (iii) in Fig. 2(a)]. Upon further decreasing the field, dipolar contrast reappears but in the reverse direction, suggesting that the vortex has been annihilated, leading to a single domain or onion state [4]. If the field is then increased from negative saturation, a nearly featureless contrast is recovered for $H_{\text{appl}} = 0$ Oe [panel (vii) in Fig. 2(a)]. This is in agreement with the vortexlike hysteresis loop of Fig. 1(b), where the remanence is zero for this branch of the loop [29]. Dipolar contrast, typical of the single domain state, is again observed at positive saturation. Figure 2(b) reveals that the magnetic reversal mode, when the applied field is perpendicular to the exchange bias direction (i.e., 90°), is drastically different. In this case, applied fields of ±550 Oe (maximum available in the MFM) are not sufficient to fully saturate the sample. Nevertheless, magnetic images show dipolar contrast, consistent with coherent rotation reversal [panels (i)–(iii)].

Figure 3 shows typical calculated hysteresis loops and the field evolution of the spin configurations, along 0° and 90°, obtained from micromagnetic simulations. The simu-

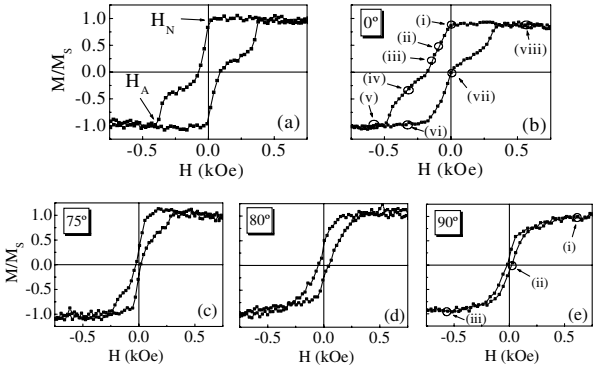

FIG. 1. Hysteresis loops of: (a) the circular dots with composition Ta/Py/Pt (i.e., without AFM); (b),(c),(d),(e) the FM-AFM dots, with composition Ta/Py/IrMn/Pt, measured with the magnetic field applied (b) along the FC direction, 0°, (c) at 75°, (d) at 80°, and (e) at 90° with respect to the FC direction. The nucleation and annihilation fields, H_N and H_A, of the vortex state are indicated in (a).

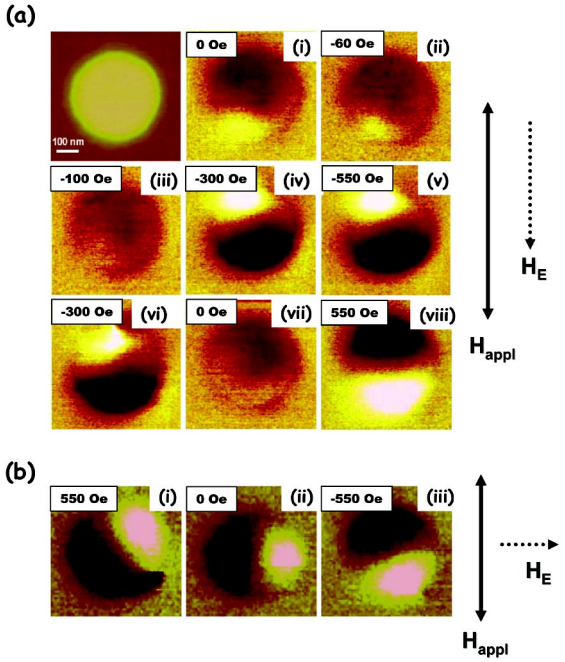

FIG. 2 (color online). In (a) the top left panel is an atomic force microscopy image of a single circular dot. The subsequent panels are MFM images acquired under different magnetic fields [as indicated in Fig. 1(b)] applied parallel to the exchange bias direction (i.e., 0°). (b) MFM images of the exchange biased dots, with the external field [as indicated in Fig. 1(e)] applied perpendicular to the exchange bias direction (i.e., 90°).

lations confirm that the magnetization reversal occurs via nucleation and annihilation of a vortex state when the field is applied along the exchange bias direction, whereas a vortex state is absent for the perpendicular direction. Actually, in the simulations, along the 90° direction and intermediate field values, the unidirectional exchange favors the formation of a so-called *S* state, where the spins in the FM tend to orient in a shape reminiscent of the letter "*S*" [4]. In general, as the magnetic field is reduced, a dot will take on a curled magnetization state to minimize stray fields at the dot edges. The simulations show that if an exchange bias field is superimposed at an angle from the applied field then the perpendicular component of the exchange bias selects a preferred edge-magnetization direction, hence resulting in the *S* state.

The experimental exchange bias loop shift H_E of the dots can be evaluated either from the two nucleation or the two annihilation fields. Figure 4(a) shows the angular dependence of H_E for the two cases, which follows closely a $H_E(\theta) = H_E(0)\cos(\theta)$ relationship. A similar angular dependence is observed for continuous Py/IrMn films [19]. As the applied field is rotated from the FC direction, both the measured nucleation and annihilation fields progressively decrease with angle, i.e., the loops become overall narrower [see Figs. 1(b) and 1(c)]. The angular dependencies of the nucleation fields, for both the descending (H_{N1}) and ascending (H_{N2}) branches of the hysteresis loops are plotted in Fig. 4(b). It is noteworthy that although H_{N2} strongly decreases with angle, H_{N1} is quite insensitive to the direction of measurement. The average nucleation field, $H_N = (H_{N1} - H_{N2})/2$, is plotted as a function of the measuring angle in Fig. 4(c), while Fig. 4(d) shows the angular dependence of the average annihilation field, H_A. As the angle θ from the exchange bias direction increases, both $H_N(\theta)$ and $H_A(\theta)$ progressively decrease with respect to $H_N(0)$ and $H_A(0)$, which are the fields necessary to nucleate/annihilate the vortex if there was no exchange bias. Indeed, as a first approximation, one can consider that the unidirectional exchange coupling with the AFM can be represented by the exchange bias field, $\vec{H}_E$. The hysteresis loops measured along the FC direction lead directly to the "real" average nucleation field of the vortex, since the applied field directly compensates the exchange bias field. If $\vec{H}_E$ is oriented at an angle from the applied external field, the vortex will nucleate when the absolute value of the effective field $\vec{H}_{\text{eff}} = \vec{H}_{\text{appl}} + \vec{H}_E$ becomes equal to the nucleation field of the vortex, $H_N(0)$ [see inset Fig. 4(c)]. Consequently, using simple geometric calculations, one can estimate H_{N1} and H_{N2} (which, to be accurate, are the external fields that need to be applied, so that $|\vec{H}_{\text{eff}}| = H_N(0)$), as follows:

$$H_{N_2^1}(\theta) = H_E(0)\cos(\theta) \mp \sqrt{H_N^2(0) - H_E^2(0)\sin^2(\theta)} \quad (1)$$

These calculated fields are plotted as lines in Fig. 4(b). In our case, since $H_N(0) \approx H_E(0)$, Eq. (1) correctly predicts that $H_{N1} \approx 0$ and is almost independent of θ. From Eq. (1), the average nucleation field, $H_N(\theta)$, is $H_N(\theta) = \sqrt{H_N^2(0) - H_E^2(0)\sin^2(\theta)}$, shown by the line in Fig. 4(c). With a similar argument one would expect $H_A(\theta) = \sqrt{H_A^2(0) - H_E^2(0)\sin^2(\theta)}$, which should be almost constant

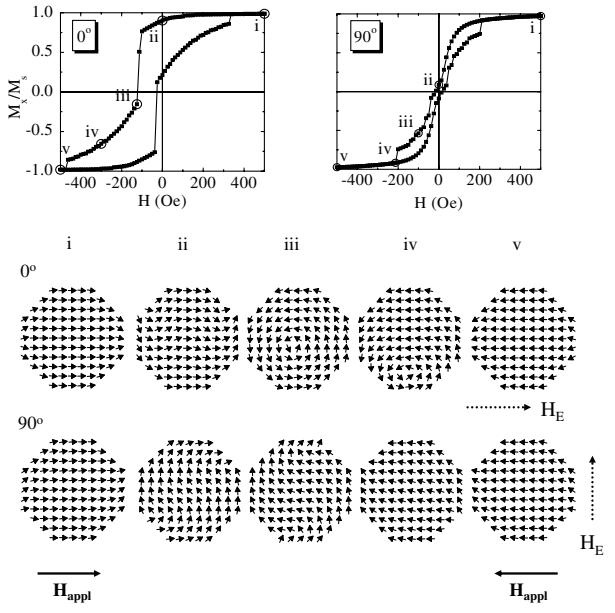

FIG. 3. Simulated hysteresis loops, measured along 0° and 90° with respect to the field cooling (i.e., exchange bias) direction, together with spin configurations corresponding to selected values of fields, as indicated in the loops.

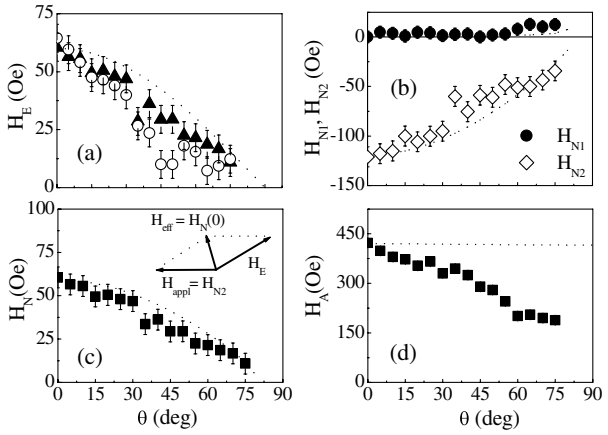

FIG. 4. Angular dependence of (a) the exchange bias loop shift, H_E, of the dots, as determined from the nucleation (▲) or the annihilation (○) fields of the ascending and descending branches of the hysteresis loops; (b) the nucleation fields for the descending and ascending branches of the hysteresis loop, H_{N1} and H_{N2}; (c) the average nucleation field, H_N; and (d) the average annihilation field, H_A. The dotted line in (a) corresponds to a $H_E\cos(\theta)$ fit, whereas the lines in (b),(c), and (d) correspond to the values obtained from the geometrical model [Eq. (1)]. The inset in (c) is a schematic representation of the vectorial sum used for the determination of the nucleation and annihilation fields.

since $H_A(0) \gg H_E(0)$. However, this simple geometrical argument does not properly account for the angular variation of $H_A(\theta)$, as can be seen in Fig. 4(d). In fact, the micromagnetic calculations suggest that the decrease of H_A from 400 to 200 Oe is correlated with changes in the intermediate magnetization structure during the reversal process. In the calculations the vortex nucleation proceeds with increasing angle first via a C, then via an S state with a tendency to nucleate two vortices, and finally for the largest angles the vortex nucleation is completely suppressed. The magnitudes of the calculated H_A at low and high angles are comparable to the experimental value; however, the exact angular dependence varies with the modeling parameters, which makes a quantitative comparison with the experimental data difficult. Equation (1) also predicts the existence of a critical angle, $\theta_C = \arcsin[H_N(0)/H_E(0)]$, beyond which the vortex nucleation does not occur. Taking into account that $H_E(0)$ is just slightly larger than $H_N(0)$, θ_C is indeed found to be close to 80°, as observed experimentally. It should also be noted that angular variations in H_N and H_A have already been reported in the literature for arrays of circular dots with strong interdot magnetostatic interactions [6,27,30], where an interaction field is superimposed on H_N and H_A, or for elliptical dots [31,32]. In the latter case, either S states or double vortices are observed when measuring along the long axis of the ellipses, whereas a C state or a single vortex are obtained along their short axis, thus evidencing that different magnetization reversal mechanisms can occur in anisotropic systems depending on the field direction [31,32]. The coupling with an AFM is in some sense similar since the exchange bias also breaks the symmetry of the circular dots in a manner analogous to the interdot interactions or the elliptical shape. For sufficiently large exchange bias fields, the FM-AFM coupling can even induce completely different magnetization reversal modes, depending on the angle of measurement. The actual reversal mechanism depends on the interplay between the different energies (i.e., magnetostatic, exchange) involved in the system. Finally, it should be noted that exchange bias is a complex phenomenon, and thus it may not be fully described by an extra field superimposed onto the applied external field. Hence, although our simple analysis provides an understandable description of the system's general behavior, the underlying microscopic mechanisms are considerably more complex, as shown, for example, by the behavior of the annihilation field.

In summary, the magnetization reversal mechanisms of circular FM-AFM dots with submicron diameter have been found to depend on the direction of the applied field. Along the exchange bias direction, the magnetization reversal occurs via vortex formation. If the magnetic field is applied at an angle to the FC direction, the measured nucleation field progressively decreases. When the magnetic field is applied beyond a critical angle, in our case $\theta_C \sim 80°$, the vortex state no longer nucleates. This is confirmed by MFM imaging together with micromagnetic simulations. Our results show that the magnetization reversal of submicron disks is significantly more complex when the magnetostatic energies have to compete with additional interactions.

Financial support from the NEXBIAS (HPRN-CT 2002-00296), the 2001-SGR-00189, the MAT-2004-01679 projects, and the U. S. DOE-BES, under Contract No. W-31-109-ENG-38 is acknowledged. We would like to thank K. Yu. Guslienko, and V. Novosad for stimulating discussions. K. B. acknowledges NSERC of Canada for financial support.

*Electronic address: jordi.sort@uab.es

[1] J. I. Martín *et al.*, J. Magn. Magn. Mater. **256**, 449 (2003).
[2] C. A. Ross, Annu. Rev. Mater. Sci. **31**, 203 (2001).
[3] P. O. Jubert and R. Allenspach, Phys. Rev. B **70**, 144402 (2004).
[4] J. K. Ha, R. Hertel, and J. Kirschner, Phys. Rev. B **67**, 224432 (2003).
[5] R. P. Cowburn *et al.*, Phys. Rev. Lett. **83**, 1042 (1999).
[6] K. Y. Guslienko *et al.*, Phys. Rev. B **65**, 024414 (2002).
[7] S. P. Li *et al.*, Phys. Rev. Lett. **86**, 1102 (2001).
[8] T. Shinjo *et al.*, Science **289**, 930 (2000).
[9] B. Dieny, Phys. Rev. B **43**, 1297 (1991).
[10] J. Nogués and I. K. Schuller, J. Magn. Magn. Mater. **192**, 203 (1999).
[11] A. E. Berkowitz and K. Takano, J. Magn. Magn. Mater. **200**, 552 (1999).
[12] R. L. Stamps, J. Phys. D: Appl. Phys. **33**, R247 (2000).
[13] M. Kiwi, J. Magn. Magn. Mater. **234**, 584 (2001).
[14] D. Mauri *et al.*, J. Appl. Phys. **62**, 3047 (1987).
[15] A. P. Malozemoff, Phys. Rev. B **35**, 3679 (1987).
[16] M. Kiwi *et al.*, Europhys. Lett. **48**, 573 (1999).
[17] P. Miltényi *et al.*, Phys. Rev. Lett. **84**, 4224 (2000).
[18] M. Fraune *et al.*, Appl. Phys. Lett. **77**, 3815 (2000).
[19] V. Baltz *et al.*, Appl. Phys. Lett. **84**, 4923 (2004).
[20] J. C. Wu *et al.*, J. Appl. Phys. **87**, 4948 (2000).
[21] J. Yu, A. D. Kent, and S. S. P. Parkin, J. Appl. Phys. **87**, 5049 (2000).
[22] A. Hoffmann *et al.*, Phys. Rev. B **67**, 220406(R) (2003).
[23] K. Liu *et al.*, Appl. Phys. Lett. **81**, 4434 (2002).
[24] Z.-P. Li *et al.*, Appl. Phys. Lett. **86**, 072501 (2005).
[25] J. Mejía-López, P. Soto, and D. Altbir, Phys. Rev. B **71**, 104422 (2005).
[26] J. I. Martín *et al.*, J. Appl. Phys. **84**, 411 (1998).
[27] V. Novosad *et al.*, Phys. Rev. B **65**, 060402 (2002).
[28] M. R. Scheinfein, LLG Micromagnetics Simulator™.
[29] Note that the weak dipolar contrast visible in Fig. 2(a) (vii) probably arises from the different measuring approaches of MFM and MOKE, i.e., while MFM is local and static, MOKE is dynamic and averages over many dots. Moreover, simulated MFM images at $H_{\text{appl}} = 0$ show also a weak dipolar contrast due to a displaced vortex.
[30] M. Natali *et al.*, J. Appl. Phys. **96**, 4334 (2004).
[31] P. Vavassori *et al.*, Phys. Rev. B **69**, 214404 (2004).
[32] X. Liu, J. N. Chapman, S. McVitie, and C. D. W. Wilkinson, J. Appl. Phys. **96**, 5173 (2004).